PCCP

Accepted Manuscript

ROYAL SOCIETY OF CHEMISTRY

www.rsc.org/pccp

Journal Name

RSCPublishing

ARTICLE

Photocontrol of Luminescent Inorganic Nanocrystals *via* an Organic Molecular Switch

Cite this: DOI: 10.1039/xoxxoooooox

Received ooth January 2012,
Accepted ooth January 2012

DOI: 10.1039/xoxxoooooox

www.rsc.org/

J. Massaad[a], Y. Coppel[b], M. Sliwa[c]*, M. L. Kahn[b]*, C. Coudret[a]*, F. Gauffre¶[d]*

A photo-controlled and quasi-reversible switch of the luminescence of hexadecylamine-coated ZnO nanocrystals (ZnO@HDA Ncs) is operated via a molecular photoswitch (dithienylethene, DTE). The interaction between the DTE switch and the ZnO@HDA Ncs is thoroughly investigated using NMR spectroscopy techniques, including DOSY and NOESY, showing that the DTE switch is weakly adsorbed at the surface of the Ncs through the formation of hydrogen bonds with HDA. Steady state and time-resolved luminescence quenching experiments show a complex behavior, related to the spatial distribution of the emitting defects in the Ncs. Analysis of the data using models previously developed for Ncs supports static quenching. Both isomeric forms (open or closed) of the DTE switch quench the Ncs emission, the efficiency being more than ten times higher for the closed isomer. The mechanism of quenching is discussed and we show that quenching occurs mainly through resonant energy transfer for the closed isomer and through electron transfer for the open one. The HDA layer mediates the quenching efficiency as only defects located near the surface are quenched.

Journal Name RSCPublishing

ARTICLE

Introduction

Photo-switchable luminescent devices are highly desirable for advanced technologies, when a spatial and temporal control of the optical state is required. Applications include reversible optical data storage and new high-resolution imaging techniques such as Photoactivated Localization Microscopy (PALM) and others.[1–7] At the molecular scale, the design of photoswitchable systems relies on the association of two components: (i) a luminescent material (either organic or inorganic) and (ii) a photochromic dye (or molecular photoswitch), this latter operating the switch of the luminescent component.[8–14] The photomodulating action of the switch can be schematically pictured as follows. Photochromic dyes generally exist under two isomeric forms. Switching from one form to the other is activated by light irradiation. When coupled to a luminescent material, the photomodulation effect results from a higher quenching efficiency of one of the isomers compared to the other. Spiropyran, spiro-naphthooxazines and dithienylethene are the most commonly used photochroms for the photocontrol of both organic and inorganic fluorophores.[12,13] In particular, dithienylethenes form a group of P-type photochroms, requiring light for both coloration and discoloration. This "conjugation switch" has been used to design molecular electronic components,[15–17] photoacids[18–20] or photocatalysts.[18] The HOMO-LUMO gap variation induces a large change in the redox properties of the two isomers,[19,21,22] and also in their quenching ability. Thus, the association of dithienylethene with luminescent material makes an attractive combination for the elaboration of photomodulated devices.[11,23,24] Whereas many organic dyads allowing photocontrol are known, the photocontrol of luminescent inorganic nanocrystals (Ncs) by an organic dye is still in its infancy.[25–29] The continuous improvements of synthesis protocols have given access to a wide variety of inorganic Ncs with always finer optical properties.[30,31] The strong motivation for using inorganic Ncs is due in part to their resistance to photobleaching, which has stimulated their interest for several applications such as sensing and biological tagging.[31,32] In particular, quantum dots have a broad excitation spectra and a narrow emission profile which can be tuned with the size of the nanocrystal, thus enabling an effective matching of their spectral properties with these of the organic acceptor for Förster Resonant Energy Transfer (FRET).

In the literature, photoluminescence (PL) quenching of Ncs by organic dyes has been most often interpreted in terms of energy transfer. We reasoned that the combination of the diacid diarylethen photoswitch[20] (DTE, Figure 1) with luminescent ZnO Ncs would be ideally suited to achieve emission photocontrol through FRET, since the absorption spectra of the closed isomer of DTE (DTE-c) overlaps with the Ncs emission whereas the open isomer does not (Figure 1a). To this aim, we synthesized ZnO Ncs with a controlled surface state, *via* an established organometallic procedure.[33] These Ncs exhibit a non-excitonic visible PL related to defect states, which was characterized in previous studies.[34] We have investigated the photo-switchable PL of solution mixtures of ZnO Ncs and DTE. Since a partial quenching of the ZnO Ncs PL was previously observed due to the substitution of the amine ligand with a more effective electron donor ligand, we decided not to bind chemically the DTE to the Ncs surface.[35] We demonstrate evidence of light-activated, quasi-reversible, *on-off* control of the luminescence of the ZnO Ncs. We show using NMR spectroscopy, including DOSY and NOESY, that DTE is transiently interacting with the ligand shell surrounding the ZnO Ncs. A deep investigation of the steady state and lifetime measurements of ZnO PL in the presence of one or of the two isomeric forms of DTE reveals that it is not governed by an energy transfer process only. Photoinduced charge transfer of electrons or holes also contribute to PL quenching and cannot be ignored.[36] Quenching experiments also show that the closed isomer of DTE has a better affinity with the ZnO@HDA Ncs than the open one. Finally, we evidence that the HDA layer limits the electron transfer and mediates FRET quenching efficiency as only defects located near the surface are quenched.

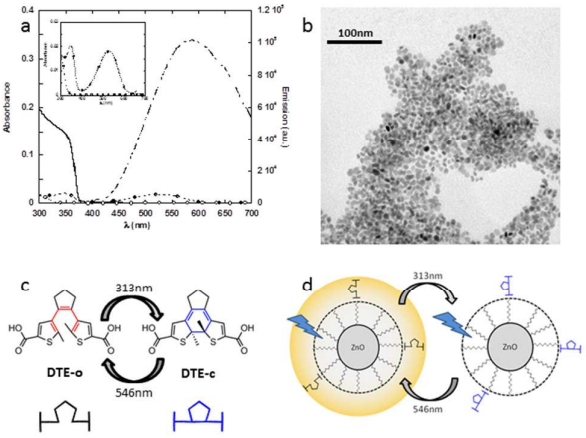

Figure 1: a) Absorbance spectra of ZnO Ncs (0.5mM of Zn atoms) (full line) and of the diarylethene moiety (0.025mM) in its open (o) and closed form (●). Dashed line: emission spectra of ZnO Ncs for λ_{exc} = 365 nm. Insert: enhanced absorbance spectra of the DTE open and closed forms. b) TEM picture of the Ncs; c) Chemical structure of the open (DTE-o) and closed (DTE-c) isomers of the diarylethene and d) photoswitching between the luminescent (yellow shell) and non luminescent state of the ZnO Ncs.

Results and discussion

Design of the photoswitchable luminescent system

Zinc oxide nanoparticles can be prepared by several routes. The classical sol-gel precipitation of ZnO from a zinc salt and a hydroxide source generally yields particles accompanied with several salts difficult to eliminate, which are believed to interact with the surface and play a role in the visible emission. We have proposed an alternative route: the hydrolysis of an

organometallic precursor, here the dialkylzinc complex [$Zn(Cy)_2$], operated at room temperature in the presence of a stabilizing ligand, here hexadecylamine (HDA).[37] This reaction is very exothermic and produces well-crystallized Ncs of controlled size and shape. Interestingly, the cyclohexane produced upon decomposition of the precursor evaporates readily with the solvent. The Ncs used in this study are roughly cylindrical (Figure 1b). From the Gaussian analysis of the size histograms, we determined their mean length (9.2 ± 2.1 nm) and mean diameter (5.7 ± 1.0 nm). In this notation, the first value corresponds to the center of the peak whereas the second one corresponds to twice the standard deviation of the Gaussian distribution or approximately 0.849 the width of the peak at half-height. The mean number of Zn (or O) atoms per particle (9200 ± 3800) can thus be estimated from the crystallographic parameters of ZnO würtzite assuming a cylindrical shape (see experimental section for details).

The photophysical properties of ZnO Ncs and of the diarylethene moieties are presented in Figure 1a. The room temperature emission spectrum of the as prepared ZnO Ncs obtained for an excitation in the UV region (see absorbance spectrum of ZnO Ncs also in Figure 1a) is dominated by a broad visible emission (maximum centered at 580 nm, *i.e.* 2.14 eV) resulting from defects, probably charged oxygen vacancies, acting as deep electron trap.[38–41] By comparison with quinine sulfate, a value of 0.28 was evaluated for the ZnO Ncs emission quantum yield. This is consistent with the value of 0.15 reported by Mulvaney et al. for smaller ZnO Ncs (3.2 nm) for which surface quenching should be stronger.[42] It is worth noting that whereas other synthesis conditions may yield nanoparticles with two distinct emissions at 440 nm and 580 nm which were interpreted as corresponding to two types of emitting defects,[34] the ZnO synthesized in this work exhibit overwhelmingly the emission at *ca* 580 nm, which will further simplify the analysis of the PL measurements. Concerning the DTE switch, the cyclization reaction from the open (DTE-o; colorless) to closed (DTE-c; colored) forms of DTE is activated by irradiation in the UV range (313 nm, 3.96 eV) and reversed by irradiation in the visible range (546 nm, 2.27 eV) (Figure 1c).

To evidence the switchable luminescence of the ZnO/DTE dyad, a THF solution of ZnO Ncs with DTE-o was irradiated at 313 nm for 10 mins and at 546 nm for 20 mins (the ring opening reaction being much less efficient than the cyclisation).[20] After each irradiation, the absorbance at 524 nm and the emission intensity (λ_{exc} = 365nm, λ_{em} = 580nm) were measured. Irradiation cycles through the open and closed states of DTE give rise to an "on/off" behavior of the solution PL (Figure 2). The first switch from the on- to the off- state resulted in an extinction of 63% of the PL. Note that after this first cycle, the on-states emit only 65% of the initial PL intensity. Meanwhile, the residual emission from the off-state becomes more significant. After the second cycle, the quenching became stable with a rate of *ca.* 33%, which compares with previous quenching experiments using DTE moieties and CdSe/ZnS QD.[27] Although we haven't looked for an in-depth analysis of the photofatigue of the system on cycling, several explanations can be proposed. i) An incomplete bleaching/coloring. Indeed, it is obvious from the absorbance monitoring, that the stationary states were not completed through cycling. Irradiation times were intentionally limited to prevent photodegradation of the DTE switch.[20] ii) It is known that diarylethene are prone to photofatigue especially over long irradiation time, and one identified path leads to an irreversible isomerization into a colored species with a UV-vis spectra very similar to the closed isomer (Supporting Information SI-1).[43] Both these hypotheses are consistent with the raise in the emission of the off-state and the persistence of a residual absorption at 524 nm despite the irradiation for 20 minutes. iii) In addition, a photodegradation of acidic forms of DTE upon UV-irradiation in the presence of ZnO was reported previously,[44] and might explain the continuous decrease of the absorbance maximum (off-state).

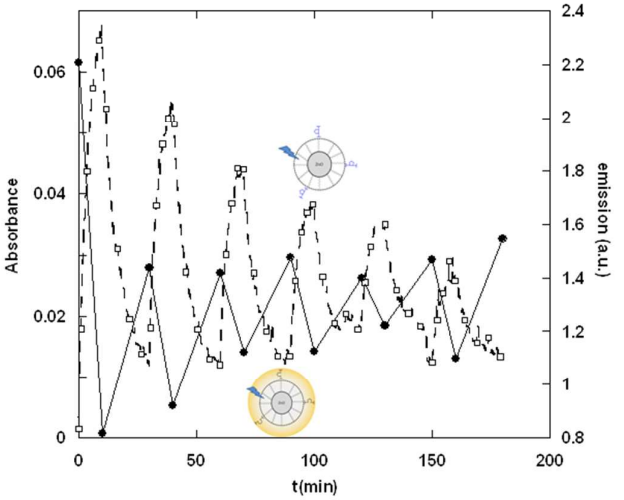

Figure 2: Spectroscopic monitoring of the ZnO/DTE Ncs, cycled through the open and closed states of DTE. (●) On-Off luminescence (λ_{exc}=365nm, λ_{em}=580); (□) absorbance at 524nm. [ZnO] = [HDA] = 0.81mM; [DTE] = 2.1 10^{-2}mM (0.026eq)

Surprisingly, the emission of ZnO Ncs was significantly quenched (*ca* 60%) on addition of the open form of DTE. Since there is no spectral overlap between DTE-o and ZnO, this result implies an electron transfer mechanism. Therefore, charge transfer quenching might also be considered for DTE-c. Comparing the DTE's absolute redox potentials with the ZnO levels allows one to estimate the electron transfer free energies and its thermodynamic feasibility (Figure 3, and SI-2). Dithienylethenes have been shown to have a rich electrochemical behaviour. In particular, it is known that the closed colored forms are easier to oxidize than their open counterpart. This is the case for the diacid used in this study, and the first oxidation redox couple of closed isomer is *ca* 500 mV more cathodic than the open isomer's one. On the other hand, ZnO Ncs are known to undergo redox processes once in their excited state.[45,46] However, as crystal's defects act as charge traps it is difficult to estimate the locus and the energy of the charge transfer. Oxygen vacancies can act as holes traps. The resulting charged defect V'_O, is lying in the middle of the band gap and is thought to be responsible in part for the observed visible emission by the recombination of the electron from the conduction band (CB) with the hole hosted in the V'_O defect.[34,47] An electron transfer from the DTE's HOMO level (located at -5.9 eV and -5.2 eV for the open and closed isomer respectively)[48] towards V'_O is thus energetically favorable. It was demonstrated previously that ZnO Ncs coated with dodecylamine can exchange electrons despite the presence

of the ligand layer.[46] This suggests that in the present case, electron transfer can also occur, however the "insulating" hexadecylamine (*ca* 20Å) layer may damp such processes.

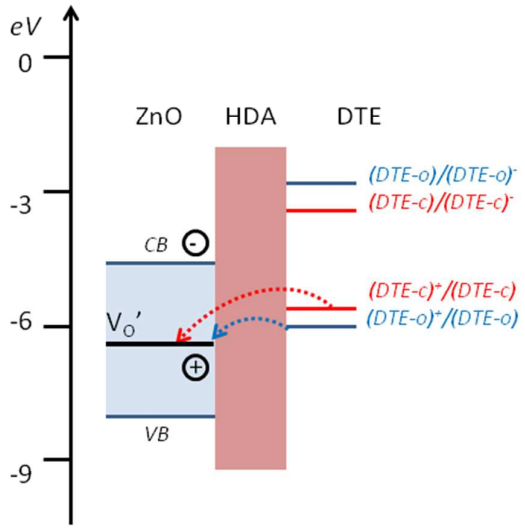

Figure 3: Energy diagram for positioning the redox couple of DTE-o and DTE-c relatively to ZnO (referenced to vacuum). Arrows represent possible electron transfers.

To better understand the quenching behavior of ZnO Ncs by DTE isomers, steady state and time resolved experiments were performed. Samples were obtained by first preparing THF solutions of DTE either in the open form or as a mixture of both isomers by irradiation and then mixing these solutions with solutions of ZnO Ncs. In the following, the mixture "closed-open" is noted DTE-c-o. Firstly, a NMR study was conducted to try to evaluate the interaction of the DTE with the ZnO@HDA Ncs, which is important to quantify precisely the quenching.

Characterization of the interaction of DTE-o with the ZnO Ncs by NMR spectroscopy.

NMR spectroscopy is emerging as a powerful technique for identifying ligands at the surface of nanoparticles.[49] A previous NMR study by our group demonstrated that the ZnO Ncs are surrounded by a complex network of the amine ligands.[50] A primary shell of ligand is constituted of a mixture of strongly bonded amines (possibly through dative coordination of the amine to Zn^{2+}) together with amines interacting less strongly, through hydrogen bonding (THF and water molecules kinetically trapped at the surface of the Ncs during the synthesis are also present). A secondary layer of ligands is weakly interacting with the first shell and exhibits a relatively fast exchange dynamics with ligands free in solution. As a whole, the thickness of the ligand layer is estimated to *ca.* 2-3 nm.[50] Following these results, an NMR spectroscopic study (including DOSY and NOESY) was achieved to investigate the interaction of DTE-o with the ZnO@HDA Ncs. In order to characterize the possible association of DTE species with HDA, association previously observed for mixtures of fatty acids and fatty amines,[50] mixtures of DTE-o and 5.4 eq. of HDA ([DTE-o] = 1.5 mM), were firstly investigated in the absence of ZnO Ncs. The significant resonance shifts (Figure 4) of the proton of DTE (-140 Hz for H/thiophene and + 50 Hz for methyls) and of HDA (+ 36 Hz and + 40 Hz for α and β protons, respectively) together with the decrease of the diffusion coefficient of both DTE-o and HDA (Table 1) evidence an interaction between these species. Such association may involve either acid carboxylic-amine moieties or carboxylate-ammonium pairs. We have shown previously that DTE-o undergoes significant UV-vis spectral changes upon ionization.[20] However no such changes were observed upon recording UV-visible spectra of DTE-HDA mixture in THF excluding the presence of carboxylate species. These results suggested the association of HDA and DTE species through hydrogen bonded complex.

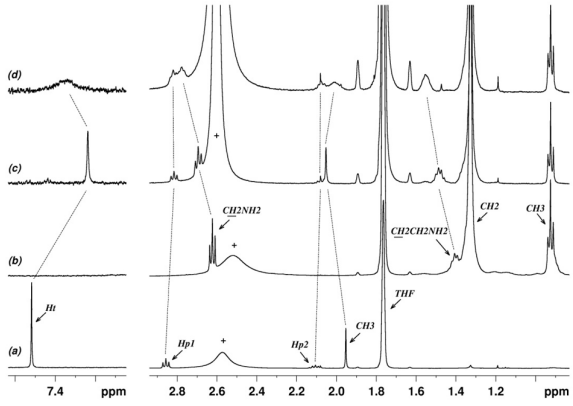

Figure 4: ^{1}H-NMR spectra in THF at 291K of DTE-o (a), of HDA (b), of HDA/DTE-o in a ratio 2/1 without (c) and with ZnO Ncs (d). Only area corresponding to the region between 7.5 and 7.3 ppm and 3.0 and 1.0 ppm are shown for clarity. Ht: thiophene proton of DTE-o; Hp1 et Hp2: cyclopentyl protons of DTE-o; +: exchangeables protons (H_2O, NH_2, COOH,…).

In the presence of ZnO Ncs, shifts and broadening of the proton resonances of both the DTE and the HDA are observed. The shifts of the protons resonance are less pronounced for the DTE (-84 Hz for H/thiophene and + 28 Hz for methyl) than for HDA (+ 78 Hz for α and + 73 Hz for β protons), while the broadenings of the signals corresponding to the thiophene and the methyl protons of DTE-o (~7.45ppm) are more important than for the methylene protons in the α and β positions of HDA. These resonances shifts and broadening are characteristic of the interaction of both DTE-o and HDA with the Ncs. The diffusion coefficients of DTE-o and HDA (Table 1) provide information about their dynamics. Experimentally, the diffusion coefficient of DTE-o in the presence of ZnO Ncs (5.3 (±0.5) $x10^{-10}$ $m^2.s^{-1}$) is only slightly modified compared to the one of DTE-o in the DTE-o/HDA mixture; but the diffusion coefficient of HDA is more impacted, with a reduction from 10.0 (±0.2) $x10^{-10}$ $m^2.s^{-1}$ down to 7.0 (±0.5) $x10^{-10}$ $m^2.s^{-1}$. For both HDA and DTE-o, only one diffusion coefficient is observed, the value of which is much larger than the one that should be observed for the Ncs (estimated to be *ca.* $D_{Ncs} \sim 0.7 \times 10^{-10}$ $m^2.s^{-1}$ for a sphere of diameter 6 nm). These results indicate that there are DTE and HDA species both interacting with the Ncs and free in solution, which are in fast exchange compared to the NMR timescale. These results are strengthened by the NOESY experiments (mixing time of 100 ms, SI-3) which exhibit negative NOEs signals for both HDA and DTE-o. According to the value of their diffusion coefficients, HDA and DTE-o should show a small but positive NOE (NOE should

vanish for a diffusion coefficient value of *ca*. Dcrossover = 4.5 10^{-10} m^2 s^{-1} on a 500 MHz NMR spectrometer).[50] These observed negative NOEs are therefore transferred NOEs due to a fast exchange (relatively to the timescale of the NMR relaxation) between adsorbed species and free species. To summarize, the NMR study showed that HDA and DTE-o interact probably as hydrogen bond species with the ZnO Ncs. This interaction is weak with a relatively fast exchange between bonded species and the ones free in solution. Taking into account the NMR data of the present work, we can reasonably picture that DTE has no direct interaction with the ZnO surface. In contrast, it interacts with HDA both in the solution and within the second layer of ligands, most probably through the formation of hydrogen bonds. A crude approximation of the maximum number of DTE molecules adsorbed per Nc can be calculated. Indeed, if $D_{DTE\text{-}o}$ and D_{free} are the observed diffusion coefficients of DTE in the presence (ZnO/HDA/DTE) and in the absence (HDA/DTE) of the Ncs respectively, then we expect: $D_{DTE\text{-}o} = x_{Ncs} D_{Ncs} + (1-x_{Ncs}) D_{free}$, where x_{Ncs} is the molecular fraction of DTE adsorbed to Ncs and D_{Ncs} the diffusion coefficient of the Ncs (0.7×10^{-10} $m^2.s^{-1}$, vide infra).[51] Since the diffusion coefficients of DTE in the presence (ZnO/HDA/DTE) and in the absence (HDA/DTE) of the Ncs are similar (within the experimental error, ca 10%) we can estimate that there are less than 4 DTE molecules adsorbed per Ncs in these conditions of concentration.[51]

	Pure sol.	DTE-o/HDA	ZnO/HDA	ZnO/HDA/DTE-o
$D_{DTE\text{-}o}$ $\times 10^{10}$ $m^2.s^{-1}$	8.1 (±0.1)	5.1 (±0.3)	-	5.3 (±0.5)
D_{HDA} $\times 10^{10}$ $m^2.s^{-1}$	12.0 (±0.4)	10.0 (±0.6)	9.5 (±0.5)	7.0 (±0.5)

Table 1: Diffusion coefficients of DTE-o and HDA in the various conditions related to our study: pure solvent (deuterated THF) ([DTE-o]= 3.1 mM, [HDA]=1.65 mM), DTE-o/HDA mixtures ([HDA] = 1.5 mM and [DTE-o]=0.28 mM) , ZnO/HDA ([ZnO] = [HDA] = 1.45 mM), ZnO/HDA/DTE-o mixtures([ZnO] = [HDA] = 1.45 mM and [DTE-o]=0.28 mM).

Steady-state and time resolved luminescence measurements.

In order to characterize the mechanism of quenching, steady state and time resolved PL studies were achieved. Figure 5 shows the steady state emission spectra of solutions of ZnO Ncs with various amounts of a DTE-o solution (Figure 5a) or of a DTE-c-o (Figure 5c) solution prepared by irradiation (DTE-c: 38%; DTE-o: 62%), and the corresponding Stern-Volmer representations (Figure 5 b and d). Note that the quenching effect of the DTE-o-c solution was corrected from the effect of the open isomer by: (i) recalculation of the DTE-c concentration in the mixture and (ii) substraction of the contribution from the open isomer's to quenching. DTE-c exhibits an efficient quenching characterized by a Stern-Volmer constant $K_{SV} = 5.3\ 10^6\ M^{-1}$. As mentioned previously, DTE-o also shows a quenching effect, however more than one order of magnitude less efficient than that of the closed isomer ($K_{SV} = 0.32\ \ 10^6\ M^{-1}$). As mentioned previously, quenching from the open isomer can only be explained by electron transfer, which is less efficient at long distance than FRET. In the present case, due to the HDA coating, the distance between DTE and ZnO Ncs was estimated to be about 2-3 nm. On increasing the concentration of DTE, quenching reaches saturation, with a residual luminescence of about 23% when only DTE-o is present whereas it is only of 13% in the presence of DTE-c. This might also be due to the fact that the number of defects accessible to FRET quenching is larger than by electron transfer. In addition, in the case of DTE-c-o the maximum of the emission spectrum shifts from 580 to 610 nm on increasing the concentration of DTE, whereas there is only a slight shift for DTE-o. This spectral shift, observed only with DTE-o-c, supports the hypothesis of quenching *via* FRET. Indeed the emission of ZnO Ncs solutions results from a distribution of individual ZnO Ncs with important differences in their spectral properties.[52] Since quenching *via* FRET is proportional to the overlap between the donor emission (ZnO) and the acceptor absorption (DTE-c, λ_{max}=546 nm), the Ncs emitting closer to 546nm will be more efficiently quenched, resulting in a spectral shift on increasing the concentration of DTE-c. In contrast, quenching by electron transfer is not expected to induce a spectral shift.

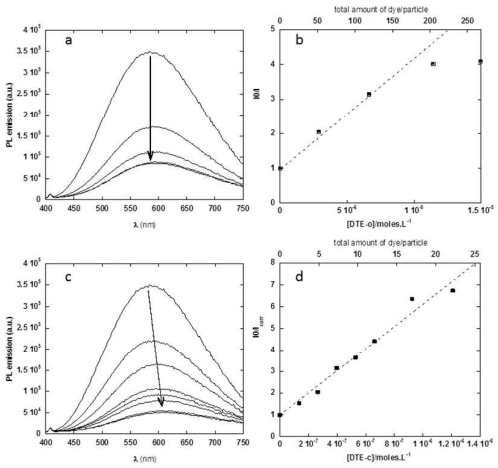

Figure 5: PL emission spectra of the ZnO Ncs with increasing amounts of a solution of a) DTE-o and b) DTE-c-o. λ_{exc}=365 nm. Stern-Volmer representation of the quenching b) by the open isomer and d) by the closed isomer after correction of the quenching by the open isomer. λ_{exc}=365 nm; λ_{em}=600nm. [ZnO] = [HDA] = 0.52mM.

PL decays of solution of ZnO Ncs in the absence or in the presence of various amount of DTE-o or DTE-c-o (mixture after bleaching) were measured (Figure 6) at 600 nm. All decays were found to be bi-exponential (deconvolved by the instrumental response function of about 10 ns) with a fast time constant of a few tens of nanoseconds and a long lived one of a few microseconds (Table 2).

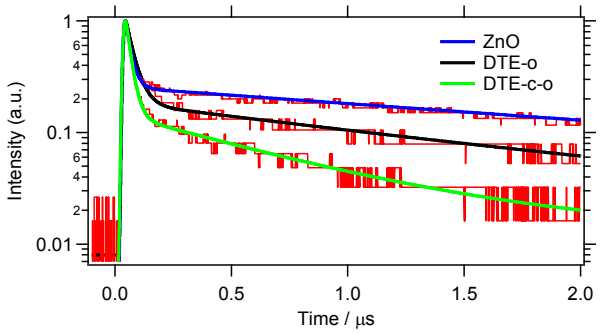

Figure 6: PL decay (logarithm intensity scale) and their bi-exponential fit at 600 nm of ZnO solutions (×) without DTE; (o) with DTE-o (0.02eq DTE); and (●) with DTE-c-o (0.02eq DTE).

	[DTE]/M	[DTE-c] / M	Bi-exponential analysis			exp{$-k_0 - \lambda_t(1-\exp(-k_{qt}t)) - \lambda(1-\exp(-k_q t))$}		
			τ_1/ µs (a_1)	τ_2 / µs (a_2)	<τ> / µs	k_0^{-1} / µs	λ_t - k_{qt}^{-1} / µs	λ - k_q^{-1} / µs
ZnO			0.023 (83%)	2.8 (17%)	2.7	2.84	1.44 - 0.036	
DTE-o	$1\ 10^{-5}$		0.035 (87%)	1.5 (13%)	1.3	2.84	1.44 - 0.036	0.85 - 0.66
DTE-o	$2\ 10^{-5}$		0.035 (88%)	1.4 (12%)	1.2	2.84	1.44 - 0.036	1.0 - 0.55
DTE-o	$3.5\ 10^{-5}$		0.032 (90%)	1.4 (10%)	1.2	2.84	1.44 - 0.036	0.98 - 0.42
DTE-c-o	$3.5\ 10^{-6}$	$1.3\ 10^{-6}$	0.028 (84%)	1.4 (16%)	1.25	2.84	1.44 - 0.036	0.98 - 1.8
DTE-c-o	$5\ 10^{-6}$	$1.9\ 10^{-6}$	0.024 (90%)	0.85 (10%)	0.67	2.84	1.44 - 0.036	1.36 – 0.36
DTE-c-o	$1\ 10^{-5}$	$3.8\ 10^{-6}$	0.022 (92%)	0.69 (8%)	0.51	2.84	1.44 - 0.036	1.56 – 0.316

Table 2. Time constants for the PL decay of ZnO Ncs in presence of DTE-o and DTE-o-c for different concentrations extracted from the fits.

The decay curve of the ZnO Ncs in the absence of DTE is independent of the wavelength. The two lifetimes extracted from the bi-exponential analysis were τ_1= 23ns and τ_2= 2.78µs respectively, which yields an averaged lifetime $<\tau_{ZnO}>$ = 2.67 µs. This average lifetime is an intensity average, calculated using the formulae, $\langle\tau\rangle = \sum_{i=1}^{i=n} a_i\tau_i^2 / \sum_{i=1}^{i=n} a_i\tau_i$. Note that similar features were observed previously for ZnO Ncs and were interpreted as resulting from a non radiative quenching by trapped states competing with the radiative decay.[41,42] In fact, a more realistic way to treat this decay is to use a static quenching model where trapped sites are fixed and randomly distributed among the nanoparticles according to a Poissonian distribution, and exhibit a limited quenching efficiency (ϕ<1). Tachiya and Mulvaney showed that the dynamics should then be described by:[53,42]

$$\frac{I}{I_0} = \exp\{-k_0 t - \lambda_t\left(1-\exp\left(-k_{qt}t\right)\right)\} \text{ (Equation 1)}$$

where k_0 represents the rate of radiative decay, and λ_t and k_{qt} the mean number of trap states by Nc and the quenching rate, respectively. Using this formalism, we found k_0= 0.352 ± 0.001 µs^{-1} (2.84 µs); λ_t= 1.44 and a transfer rate to the trap states of k_{qt} = 27.6± 0.2 µs^{-1} (0.036 µs), which compares remarkably well with the values found previously by Mulvaney (k_0= 1.7 µs^{-1}; λ_t =1.98 and k_{qt} = 39 µs^{-1}).[42]

On addition of DTE, the long lifetime is shortened whereas the short one remains unaffected. Such a decrease in lifetime is usually interpreted in terms of a dynamic quenching, involving the collision between the donor and the acceptor species. However in the present case, the quenching rate constants calculated using the Stern-Volmer plot ($k= K_{SV}/<\tau_{ZnO}>$) are equal to 1.2 10^{11} M^{-1}.s^{-1} and 2.0 10^{12} M^{-1}.s^{-1} for the open and closed form, respectively. These values are significantly higher than the maximum value expected from the diffusion-controlled bimolecular encounter rate, $k_{diff} \sim 5.10^{10}$ M^{-1}.s^{-1}, calculated from Smoluchowski's equation (see SI-4 for details of the calculation). This result rules out the possibility of dynamic quenching, and suggests that a more detailed model of static quenching should be considered. Going back to the formalism proposed by Tachiya and Mulvaney (Equation 1) and assuming also a Poissonian distribution for the DTE molecules, the quenching is given by:

$$\frac{I}{I_0} = \exp\{-k_0 - \lambda_t\left(1-\exp\left(-k_{qt}t\right)\right) - \lambda\left(1-\exp\left(-k_q t\right)\right)\}$$
(Equation 2)

λ being the average number of dyes per Nc. The emission decay curves were fitted using Eq. 2, by adjusting the parameters corresponding to quenching from the dye (λ, κ_q) and keeping constant the parameters found previously for the Ncs emission (k_0, λ_t, κ_{qt}) (Table 2). Note that Eq. 2 implicitly assumes that there is only one type of dye quencher, with a single quenching rate, κ_q. As mentioned previously, the quenching efficiency of the open form is far below that of the closed form. Consequently, considering only the closed form in the fit seems reasonable. However, due to the spatial distribution of the emitting states within the Ncs, one might expect different quenching rates, resulting from different dye-emitter distances. In addition, the decay curves exhibit a rather poor signal to noise ratio, and only two characteristic times are clearly observable. Therefore, the values λ and κ_q should be considered with caution. Having this in mind, all PL decays were fitted in the saturation regime (high dye concentration, Fig. 4), and we find that the mean number of adsorbed dye, λ is close to 1, consistently with NMR results. Regarding the quenching rate constant, since no simple model can be drawn, we decided to estimate it from the average lifetime at saturation (Equation 3):

$$k_q = \frac{1}{<\tau>} - \frac{1}{<\tau_0>} \text{ (Equation 3)}$$

where <τ> and $<\tau_0>$ are the decay times of Ncs in the presence and the absence of the quencher respectively. The rate constants calculated using this equation are k_q-o~0.47µs^{-1} and k_q-c~1.58 µs^{-1} for the open (3.5 10^{-5}M) and closed (1 10^{-5}M) isomer respectively (Table 2). These values are, in fact, very close to that obtained using Eq 2. and 2 orders of magnitude smaller than the values reported in the literature for dyes in direct interaction with the surface of ZnO Ncs.[42] This discrepancy is most probably due to the HDA layer separating the DTE switch from the Ncs surface. Furthermore, whereas complete quenching of the fast and slow components was observed in the case of the direct complexation of the dyes onto the ZnO Ncs, in the present case the distance from DTE to ZnO Ncs decreases the efficiency of the quenching which becomes slower compared to the quenching by trapped states. This explains that only the long component is affected.

For cases of static quenching, an apparent association constant, K_a, between ZnO and DTE can be determined from the steady state PL measurements, using:[54,36]

$$\frac{I_0}{I_0 - I} = \frac{I_0}{I_0 - I'} + \frac{I_0}{K_a(I_0 - I')[DTE]} \text{ (Equation 4)}$$

where I_0 and I are the measured PL intensities in the absence and in the presence of DTE and the parameter I' corresponds to the PL due to the complex only. The apparent association constant determined from the slope of the best linear fit of $I_0/(I_0-I)$ as a function of the reciprocal dye concentration (Figure SI-5) is one order of magnitude lower for DTE-o than for DTE-c (0.27±0.02 10^6 M^{-1} and 4.2 ±0.2 10^6 M^{-1}, respectively). This result confirms that the effect of the open

isomer (DTE-o) can be neglected in the analysis of the quenching by the DTE-o-c mixture. Since, the NMR results show that the dye is interacting with the amine ligand *via* hydrogen bonds, these apparent adsorption constants are related to the formation of such hydrogen bonds. Such a difference in the reactivity of the open and closed isomers of DTE was observed previously in their pK_a values.[20]

As mentioned previously, even though electron transfer can occur also for the closed isomer, FRET is faster and dominates the quenching process. It is then possible to calculate an efficiency for FRET transfer (ϕ_{FRET}) using Equation 5a and the average lifetime at saturation. A value of 81% is found which compares very well with that from steady state measurements (85%). A Förster radius of R_0 = 30 Å was calculated from these spectral features of the {DTE-c; ZnO-Nc} pair (see SI-6 for details) and an efficiency of 81% lead to a distance (r) between DTE-c and ZnO Ncs of about 25 Å. This compares with the estimated thickness of the HDA layer (~2-3 nm) and validate our hypothesis of FRET quenching from DTE-c.

$$\varphi_{FRET} = 1 - \frac{<\tau>_{DTEc-o}}{<\tau>_{ZnO}} \quad \text{(Equation 5a)} \qquad \text{and}$$

$$\varphi_{FRET} = \frac{1}{1+\left(\frac{r}{R_0}\right)^6} \quad \text{(Equation 5b)}$$

Conclusions

A photochromic diarylethene was used to switch reversibly the luminescence emission of ZnO@HDA Ncs. The amplitude of the photomodulation compares to previous studies involving QDs,[27] even though in this case the DTE switch was not covalently conjugated to the Ncs. This non covalent strategy allows one to easily vary the ratio of molecular switch per particle and to investigate the quenching efficiency of the switch. The NMR data show that DTE binds to the HDA layer through hydrogen bonds. A thoroughly analysis of lifetime experiments was achieved using dynamic and static models. We demonstrate that whereas DTE-o partially quenches the emission of ZnO Ncs through electron transfer, the FRET process is dominant in the isomer mixture obtained after photocyclisation. We find that the luminescence of the defect states is efficiently quenched (~85%) by DTE-c for a mean value of 1 DTE/particle or lower. The residual emission is attributed to unquenched defects. Indeed, from the comparison of the Förster radius for the considered acceptor/donor pair with the thickness of the HDA coating, it is clear that the dithienylethene switch quenches only emitting defects located close to the Ncs surface. Finally, the combined use of stationary, time-resolved photoluminescence techniques and NMR shows that FRET occurs between emitting defects localized at or close to the surface, and the DTE switch. This study suggests that different depths within the Ncs could be probed using ligands of different lengths. Future studies will be required to investigate precisely the in-depth location of the surface defects combined with ultrafast experiments to probe also the ultrafast deactivation of the ZnO Ncs from trapped states. We believe that the design of luminescent nanoparticles coupled with non grafted dyes interacting from a distance (that could be controlled by the thickness of the ligand layer) could be generalized to avoid strong electron transfer and provide an efficient control of the luminescence.

.

Experimental

Materials Commercially available THF was purified by distillation or by column drying before use as solvent for the synthesis or sample dilution of the ZnO Ncs.

Synthetic Procedures.

The synthesis of the diarylethene moieties was reported in details elsewhere.[20] Mixtures of open and closed form were prepared by irradiating vertically within a quartz cuvette the DTE-o solution with a 200W high-pressure mercury lamp equipped with interference filters (the optical path of the vertical irradiation was 2.5cm). The synthesis of the Zn precursor and of the ZnO Ncs were performed as described previously with other alkylamine ligands.[55] Here, a 6mL THF solution of dicyclohexyl zinc (57.9 mg, 0.25 mmoles) and 1eq. of hexadecylamine, prepared in a glove box, was treated with 2 eq. of water under inert atmosphere. The resulting transparent reaction mixture, which solidifies upon cooling, was used as stock solution and stored under argon in the dark.

TEM.

TEM samples were prepared by slow evaporation of droplets of colloidal solution to be analyzed deposited on carbon supported copper grids. The experiments were performed on a JEOL 1011 operating at 100 kV. The nanoparticle size-distribution was determined using Image-J software on magnified TEM images. A total of 1200 Ncs was measured from which the mean length, diameter and the standard deviations were extracted, using a Gaussian statistic. The volume of each of the 1200 Ncs was calculated assuming a cylindrical shape. From the mean volume value (218.2 ±8.84 nm^3) and the parameters (a= 3.24992Å and c = 5.20658 Å) of the ZnO Würtzite hexagonal lattice, we estimated the mean number of atoms per particle (9200) and the mean number of Zn atoms at the surface (1100).

Preparation of the ZnO and DTE mixtures.

The THF solutions of ZnO Ncs were gently centrifugated to eliminate any aggregate then diluted to reach an absorbance of 0.2 at 340 nm. (The absence of baseline drift (due to light scattering) can be used to check the quality of the dispersion). Mixtures of DTE and ZnO were obtained by adding small volumes of a concentrated DTE solution. All the mixtures were left to equilibrate for 12 hours before measurement. For all photoluminescence studies, the reaction mixture containing the particles was diluted until the absorbance at the edge-band was about 0.2 at 340 nm. This was found to correspond to a total zinc concentration of 0.52 mM, or in terms of Ncs concentration [Nc] = 5.7 10^{-5} mM.

On-Off switching

Cycling experiments were achieved by irradiating alternatively the mixture of ZnO-DTE at 313 nm for 600s (coloration

wavelength of the DTE-o) then at 546 nm for 1200s (discoloration wavelength of the DTE-c).

NMR

Samples were prepared as previously described, but after the 12 hrs equilibration time, the solvent was removed under vacuum and replaced by THF-d^8. ^{1}H-NMR experiments were recorded on a Bruker Avance 500 spectrometer equipped with a 5 mm triple resonance inverse Z-gradient probe. All chemical shifts are relative to TMS. All diffusion measurements were made using the stimulated echo pulse sequence with bipolar gradient pulses, at T = 291K in THF-d^8. The 2D-NOESY measurements were done with a mixing time of 100 ms.

Steady State Absorption

absorption spectra were recorded on a HP 8451 diode array spectrophotometer. All solutions were prepared by weighting to avoid error of volumetric devices.

Steady State PL

A PSS solution of DTE in THF, noted DTE-c-o ([DTE-c-o]=0.853 10^{-3}M 80:20 c:o), was prepared separately by irradiation at 313 nm for 600 s. Then mixtures of ZnO/ DTE-c-o with different concentrations DTE-c-o were prepared in anhydrous THF. All steady state emission spectra were recorded in quartz cells (1 cm optical path length) using a Jobin–Yvon spectrofluorometer. The excitation was performed at 365 nm and emission was measured at 580 nm. All the spectra are automatically corrected from the apparatus response. The spectral resolution of the slits was 2 nm. Corrections to the inner-filter effect were found to be neglictible.[50]

PL decay

For photoluminescence time decay experiments, a nano-microsecond transient absorption experiments were used. Excitation pulses at 365 nm (8 ns, 1 mJ) were provided by a 10-Hz Continuum Panther Ex OPO laser. The emitted light was collected from 450 nm to 700 nm at 90° dispersed by a monochromator (Horiba Jobin-Yvon, iHR320) and analyzed with a photomultiplier (R1477-06, Hamamatsu) coupled to a digital oscilloscope (LeCroy 454, 500 MHz). Synchronization of excitation pulses and acquisition time was secured with PCI-6602 8 Channel counter/timer (National Instruments). Samples were contained in a quartz cell (10×10 mm^2 section) at an adjusted concentration to get an absorption value of about 0.1 at the pump excitation wavelength. The experiment was controlled by a home-made software written in LabView environment. The recorded traces were averaged for several pulses and repeated for different wavelengths. The deconvolution of the individual decays with experimentally measured instrument response function (IRF) lead to 4 ns time resolution. Single wavelengths as well as global analyses of the luminescence data were performed using Igor Pro 6.20.

Acknowledgements

This work was funded by the CNRS. J.M. thanks the MESR for a grant and CNRS The authors thank Dr. J-C. Micheau for fruitful discussions.

Supporting Information Available

Irreversible Isomerization of DTE (SI-1); Photoelectrochemisty of ZnO and DTE (SI-2); NOESY (SI-3); Calculation of diffusional encounter rate (SI-4); ZnO-DTE association constant (SI-5); Förster distance for the ZnO Nc-DTE pair (SI-6). This material is available free of charge *via* the Internet at http://pubs.acs.org.

Notes and references

[a] Laboratoire des interactions moléculaires, réactivité chimique et photochimique UMR5623 CNRS and Université de Toulouse-Université P. Sabatier 118 route de Narbonne 31062 Toulouse – France..
[b] Laboratoire de Chimie de Coordination UPR8241 CNRS 205, route de Narbonne 31077 - Toulouse cedex 04 – France..
[c] Laboratoire de Spectrochimie Infrarouge et Raman, Université Lille Nord de France, Lille1, LASIR, F-59655 Villeneuve d'Ascq, CNRS-UMR 8516 – France..
[d] Institut des Sciences Chimiques de Rennes, UMR 6226 CNRS, Université Rennes 1, Campus Beaulieu, CS 74205, 35042 Rennes Cedex –France.

Electronic Supplementary Information (ESI) available: [Irreversible Isomerization of DTE (SI-1); Photoelectrochemisty of ZnO and DTE (SI-2); NOESY (SI-3); Calculation of diffusional encounter rate (SI-4); ZnO-DTE association constant (SI-5); Förster distance for the ZnO Nc-DTE pair (SI-6).]. See DOI: 10.1039/b000000x/

1. G. U. Nienhaus, *Angew. Chem. Int. Ed.*, 2012, **51**, 1312–4.
2. S. Luo, K. Chen, L. Cao, G. Liu, Q. He, G. Jin, D. Zeng, and Y. Chen, *Opt. Express*, 2005, **13**, 3123–3128.
3. B. Huang, H. Babcock, and X. Zhuang, *Cell*, 2010, **143**, 1047–1058.
4. S. T. Hess, T. P. K. Girirajan, and M. D. Mason, *Biophys. J.*, 2006, **91**, 4258–72.
5. S. Hess, T. Gould, M. Gunewardene, J. Bewersdorf, and M. Mason, *Methods Mol. Biol.*, 2009, **544**, 483–522.
6. T. Gould, V. Verkhusha, and S. Hess, *Nat. Protoc.*, 2009, **4**, 291–308.
7. Z. Tian and A. D. Q. Li, *Acc. Chem. Res.*, 2013, **46**, 269–79.
8. R. Klajn, J. F. Stoddart, and B. Grzybowski, *Chem. Soc. Rev.*, 2010, **39**, 2203–37.
9. A. Credi, *New J. Chem.*, 2012, **36**, 1925–1930.
10. Z. Tian, W. Wu, and A. Li, *ChemPhysChem*, 2009, **10**, 2577–2591.

11. R. Sanchez, R. Gras-Charles, J. L. Bourdelande, G. Guirado, and J. Hernando, *J. Phys. Chem. C*, 2012, **116**, 7164–7172.

12. E.-M. Lee, S.-Y. Gwon, Y.-A. Son, and S.-H. Kim, *Spectrochim. Acta. A. Mol. Biomol. Spectrosc.*, 2012, **97**, 699–702.

13. L. Zhu, M.-Q. Zhu, J. K. Hurst, and A. D. Q. Li, *J. Am. Chem. Soc.*, 2005, **127**, 8968–70.

14. T. B. Norsten and N. R. Branda, *J. Am. Chem. Soc.*, 2001, **123**, 1784–5.

15. S. Fraysse, C. Coudret, and J. Launay, *Eur. J. Inorg. Chem.*, 2000, 1581–1590.

16. N. Katsonis, T. Kudernac, M. Walko, S. van der Molen, B. J. van Wees, and B. L. Feringa, *Adv. Mater.*, 2006, **18**, 1397–1400.

17. N. Battaglini, H. Klein, C. Hortholary, C. Coudret, F. Maurel, and P. Dumas, *Ultramicroscopy*, 2007, **107**, 958–62.

18. H. D. Samachetty, V. Lemieux, and N. R. Branda, *Tetrahedron*, 2008, **64**, 8292–8300.

19. G. Guirado, C. Coudret, M. Hliwa, and J.-P. Launay, *J. Phys. Chem. B*, 2005, **109**, 17445–59.

20. J. Massaad, J.-C. Micheau, C. Coudret, R. Sanchez, G. Guirado, and S. Delbaere, *Chemistry*, 2012, **18**, 6568–75.

21. W. R. Browne, J. J. de Jong, T. Kudernac, M. Walko, L. N. Lucas, K. Uchida, J. H. van Esch, and B. L. Feringa, *Chemistry*, 2005, **11**, 6414–29.

22. W. R. Browne, J. de Jong, T. Kudernac, M. Walko, L. N. Lucas, K. Uchida, J. H. van Esch, and B. L. Feringa, *Chemistry*, 2005, **11**, 6430–41.

23. T. Fukaminato, T. Doi, N. Tamaoki, K. Okuno, Y. Ishibashi, H. Miyasaka, and M. Irie, *J. Am. Chem. Soc.*, 2011, **133**, 4984–90.

24. J. Chan, W. Lam, H.-L. Wong, N. Zhu, W.-T. Wong, and V. Yam, *J. Am. Chem. Soc.*, 2011, **133**, 12690–705.

25. I. L. Medintz and H. Mattoussi, *Phys. Chem. Chem. Phys.*, 2009, **11**, 17–45.

26. Z. Erno, I. Yildiz, B. Gorodetsky, F. Raymo, and N. R. Branda, *Photochem. Photobiol. Sci.*, 2010, **9**, 249–53.

27. S. Díaz, G. Menendez, M. Etchehon, L. Giordano, T. Jovin, and E. Jares-Erijman, *ACS Nano*, 2011, **5**, 2795–2805.

28. S. Díaz, L. Giordano, T. Jovin, and E. Jares-Erijman, *Nano Lett.*, 2012, **12**, 3537–44.

29. M. Liras, M. González-Béjar, and J. C. Scaiano, *Phys. Chem. Chem. Phys.*, 2010, **12**, 9757–62.

30. N. Bigall, W. Parak, and D. Dorfs, *Nano Today*, 2012, **7**, 282–296.

31. G. D. Scholes, *Adv. Funct. Mater.*, 2008, **18**, 1157–1172.

32. F. Yang, C. Jin, S. Subedi, C. L. Lee, Q. Wang, Y. Jiang, J. Li, Y. Di, and D. Fu, *Cancer Treat. Rev.*, 2012, **38**, 566–79.

33. M. L. Kahn, A. Glaria, C. Pages, M. Monge, L. Saint Macary, A. Maisonnat, and B. Chaudret, *J. Mat. Chem.*, 2009, **19**, 4044–4060.

34. M. L. Kahn, T. Cardinal, B. Bousquet, M. Monge, V. Jubera, and B. Chaudret, *ChemPhysChem*, 2006, **7**, 2392–7.

35. S. Fortuny, G. Spataro, A. Dazzazi, F. Gauffre, and M. L. Kahn, *submitted*, 2014.

36. S. Cui, T. Tachikawa, M. Fujitsuka, and T. Majima, *J. Phys. Chem. C*, 2010, 1217–1225.

37. M. L. Kahn, M. Monge, V. Collière, F. Senocq, A. Maisonnat, and B. Chaudret, *Adv. Funct. Mater.*, 2005, **15**, 458–468.

38. H. Zeng, G. Duan, Y. Li, S. Yang, X. Xu, and W. Cai, *Adv. Funct. Mater.*, 2010, **20**, 561–572.

39. A. Djurišić, W. Choy, V. Roy, Y. Leung, C. Kwong, K. Cheah, T. Gundu Rao, W. Chan, H. Fei Lui, and C. Surya, *Adv. Funct. Mater.*, 2004, **14**, 856–864.

40. V. Ischenko, S. Polarz, D. Grote, V. Stavarache, K. Fink, and M. Driess, *Adv. Funct. Mater.*, 2005, **15**, 1945–1954.

41. A. van Dijken, E. Meulenkamp, D. Vanmaekelbergh, and A. Meijerink, *J. Phys. Chem. B*, 2000, **104**, 4355–4360.

42. G. Beane, A. Morfa, A. Funston, and P. Mulvaney, *J. Phys. Chem. C*, 2012, **116**, 3305–3310.

43. D. Mendive-Tapia, A. Perrier, M. Bearpark, M. Robb, B. Lasorne, and D. Jacquemin, *Phys. Chem. Chem. Phys.*, 2014, **16**, 18463–71.

44. S. Remy, S. M. Shah, C. Martini, G. Poize, O. Margeat, A. Heyndericxx, J. Ackermann, and F. Fages, *Dye. Pigment.*, 2011, **89**, 266–270.

45. J. Yu and X. Yu, *Environ. Sci. Technol.*, 2008, **42**, 4902–7.

46. R. Hayoun, K. Whitaker, D. Gamelin, and J. Mayer, *J. Am. Chem. Soc.*, 2011, **133**, 4228–31.

47. S. Lima, F. Sigoli, M. Jafelicci Jr, and M. Davolos, *Int. J. Inorg. Mater.*, 2001, **3**, 749–754.

48. J. Massaad, J.-C. Micheau, C. Coudret, C. L. Serpentini, and G. Guirado, *Chemistry*, 2013, **19**, 12435–45.

49. A. J. Morris-Cohen, M. Malicki, M. D. Peterson, J. W. J. Slavin, and E. Weiss, *Chem. Mater.*, 2012, **25**, 1155–1165.

50. Y. Coppel, G. Spataro, V. Collière, B. Chaudret, C. Mingotaud, A. Maisonnat, and M. L. Kahn, *Eur. J. Inorg. Chem.*, 2012, 2691–2699.

51. Y. Coppel, G. Spataro, C. Pagès, B. Chaudret, A. Maisonnat, and M. L. Kahn, *Chemistry*, 2012, **18**, 5384–93.

52. A. Layek, S. De, R. Thorat, and A. Chowdhury, *J. Phys. Chem. Lett.*, 2011, **2**, 1241–1247.

53. S. Sadhu, M. Tachiya, and A. Patra, *J. Phys. Chem. C*, 2009, **113**, 19488–19492.

54. P. V Kamat and B. Patrick, *J. Phys. Chem*, 1992, **96**, 6829–6834.

55. M. Monge, M. L. Kahn, A. Maisonnat, and B. Chaudret, *Angew. Chem. Int. Ed.*, 2003, **42**, 5321–4.

